Journal of Chromatography A, 1218 (2011) 5071–5078

Contents lists available at ScienceDirect

Journal of Chromatography A

journal homepage: www.elsevier.com/locate/chroma

Zonal rate model for stacked membrane chromatography. I: Characterizing solute dispersion under flow-through conditions☆

Patrick Francis[a], Eric von Lieres[b,*], Charles A. Haynes[a,**]

[a] Michael Smith Laboratories and the Department of Chemical and Biological Engineering, University of British Columbia, Vancouver V6T 1Z4, Canada
[b] Institut für Biotechnologie 2, Forschungszentrum Jülich GmbH, 52425 Jülich, Germany

ARTICLE INFO

Article history:
Received 29 October 2010
Received in revised form 21 February 2011
Accepted 9 May 2011
Available online 14 May 2011

Keywords:
Chromatography
Ion-exchange chromatography
Membrane chromatography
Dispersion
Protein purification
Hydrodynamics
Mass transfer

ABSTRACT

Conventional models of both packed-bed and stacked-membrane chromatography typically attribute elution band broadening to non-idealities within the column. However, when the column length to diameter ratio is greatly reduced, as in stacked-membrane chromatography, variations in solute residence times within the feed-distribution (inlet) and eluent-collection (outlet) manifolds can also contribute to band broadening. We report on a new zonal rate model (ZRM) for stacked-membrane chromatography that improves on existing hold-up volume models that rely on one plug-flow reactor and one stirred-tank reactor in series to describe dispersion of solute during transport into and out of the column. The ZRM radially partitions the membrane stack and the hold-up volumes within the inlet and outlet manifolds into zones to better capture non-uniform flow distribution effects associated with the large column diameter to height ratio. Breakthrough curves from a scaled-down anion-exchange membrane chromatography module using ovalbumin as a model protein were collected at flow rates ranging from 1.5 to 20 mL min^{-1} under non-binding conditions and used to evaluate the ZRM as well as previous models. The ZRM was shown to be significantly more accurate in describing protein dispersion and breakthrough. The model was then used to decompose breakthrough data, where it was found that variations in solute residence time distributions within the inlet and outlet manifolds make the dominant contribution to solute dispersion over the recommended range of feed flow rates. The ZRM therefore identifies manifold design as a critical contributor to separation quality within stacked-membrane chromatography units.

1. Introduction

Packed-bed chromatography has remained a cornerstone of industrial and therapeutic protein purification for over a half century due to its good capacity and outstanding resolving capability. However, cost and throughput concerns associated with conventional preparative-scale chromatography, due in part to mass transfer resistances within the columns (particularly intra-pore diffusion resistances), have motivated the development of alternative purification technologies offering higher rates of mass transfer while maintaining high binding capacities and resolving power. One such technology is membrane chromatography, which is gradually gaining industrial acceptance as an attractive alternative to packed bed chromatography for the capture and downstream processing of protein products [1–3]. The interconnected pore architecture of the stacked or monolithic membrane column allows solutes to be convected across binding sites. Mass transfer is therefore enhanced, limited primarily by the rate of film diffusion or, most often, the intrinsic adsorption kinetics of the protein–sorbent complex [4]. By greatly reducing diffusion limited transport, membrane chromatography offers the well-documented potential [5–7] to increase throughput and performance provided the column design meets capacity and resolution requirements.

In most commercially available membrane chromatography units, the membranes are either axially stacked or spirally wound in order to achieve sufficient capacities [4,2,8]. To date, membrane chromatography modules with axial flow have proven more suitable for miniaturization. As a result, they provide a more easily scaled-down path to analysis and design of a particular separation provided an appropriate model is available. Several modeling approaches exist for the quantitative description of breakthrough curves from membrane chromatography modules. Most are based on a combination of the continuity equation and a kinetic equation describing protein binding and desorption [e.g. 10–14], hereafter referred to as the 1D rate theory of chromatography. Some of these models also account for dispersion in external hold-up volumes

☆ Presented at the 30th International Symposium on Proteins, Peptides and Polynucleotides (ISPPP), Bologna, Italy, 5–8 September 2010.

* Corresponding author.
** Corresponding author. Tel.: +1 604 822 5136; fax: +1 604 822 2114.
E-mail addresses: e.von.lieres@fz-juelich.de (E. von Lieres), israels@msl.ubc.ca (C.A. Haynes).

0021-9673/$ – see front matter © 2011 Elsevier B.V. All rights reserved.
doi:10.1016/j.chroma.2011.05.017

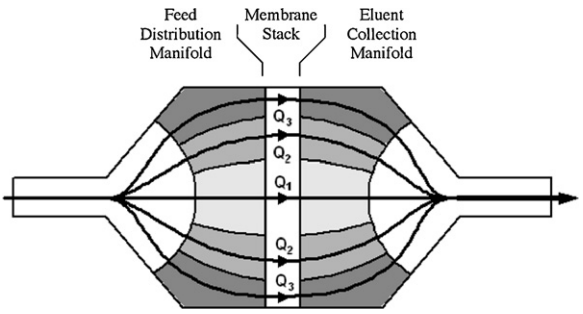

Fig. 1. Representative path lengths for solute flow within a stacked-membrane chromatography module possessing both axial and radial flow components within the feed distribution and eluent collection manifolds. Each shaded area indicates a radially defined zone in the manifold offering a distinct solute residence time, with the length of the flow line through the zone reflecting the time. Q_i represents the flow rate through zone *i*.

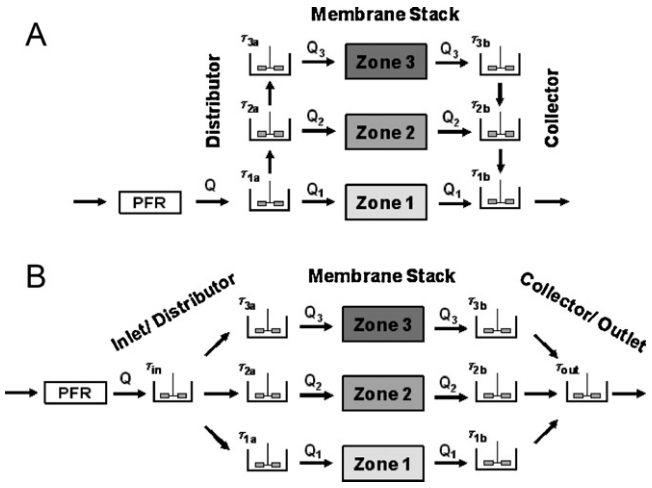

Fig. 2. Stirred tank and membrane network representation of a stacked-membrane chromatography module with (A) standard and (B) diagonal flow distribution and collection.

(which can make up, particularly in smaller modules, a large percentage of the total fluid-contacting volume) through the inclusion of a plug flow reactor (PFR) in series with a continuous stirred tank reactor (CSTR) [14–16]. Roper and Lightfoot [17] expanded on this concept to more accurately model all hold-up effects by placing a second PFR/CSTR sequence after the membrane stack in an attempt to account for solute dispersion within the eluent-collection (outlet) manifold.

However, it has now been shown that models that utilize a linear PFR/CSTR sequence either before or on both sides of the standard 1D rate theory of chromatography are not generally sufficient for quantitative reproduction of breakthrough curves from axial flow modules [18–21]. The failure of these models can arise, at least in part, from an oversimplified treatment of transport and binding processes within the membrane stack, as evidenced by the recent work of Sarti and coworkers [14] who improved prediction of breakthrough by utilizing a bi-Langmuir isotherm to account for heterogeneities in the binding energy of the sorbent. In addition, previous studies [17,22,23] of flow within different commercially available membrane chromatography units have shown that the average path length through the centerline of the feed-distribution (inlet) manifold is significantly shorter than through outer regions of the manifold, as illustrated in Fig. 1. Column loading therefore does not occur in the desired plug-flow manner, resulting in solute breakthrough from the centerline of the membrane prior to the saturation of binding sites in the outer radial positions of the membrane stack, even when the axial flow rate is constant and invariant of the radial position. This source of solute dispersion must also be properly described to realize an accurate model-based description of stacked-membrane chromatography.

In this work, we derive and evaluate a new model for membrane chromatography that specifically accounts for non-uniform radial flow distributions within the inlet and outlet manifolds. The zonal rate model (ZRM) radially partitions the external hold-up volumes and membrane stack into virtual zones. This partitioning allows for the independent treatment of solute dispersion within the hold-up volumes of each zone and therefore offers the potential to better capture the effect of the variable path lengths illustrated in Fig. 1. The ZRM is first compared to experimental data to determine the zonal configuration that best describes the dispersion of a model protein (ovalbumin) through a commercially available stacked-membrane ion-exchange chromatography module. The model is then used to decompose the observed dispersion to determine the magnitude of each contribution. All experiments and associated model calculations are performed under flow-through conditions to eliminate dispersion effects related to protein binding and desorption that might confound our efforts to characterize and model non-idealities associated with the column hold-up volumes. These results therefore build on our recent work performed on a simpler flat-sheet membrane unit for which an analytical solution to the tank network was possible, in part because dispersion in the membrane was neglected [24].

2. Theory

2.1. ZRM model description

In its most general form, the ZRM radially partitions a stacked-membrane chromatography column (hold-up volumes and membrane stack inclusive) into any number *n* of zones as illustrated in Fig. 1. There are then *n* membrane zones preceded by *n* feed distributor zones and followed by *n* eluent collector zones. The membrane stack is considered homogeneous in its properties, but is subject to different initial conditions at the membrane inlet within each zone due to differences in solute residence times within the associated zones of the feed distributor. Mobile and stationary phase composition therefore depend on the zone in addition to their typical dependence on axial position and time.

Configuration of the zones can be achieved in a number of ways. For the illustrative case where *n* is taken to be 3, Fig. 2A shows one possible arrangement of the virtual hold-up zones for modules that possess both axial and radial flow components within the inlet and outlet manifolds. Radial flow in this configuration, hereafter referred to as the "standard" configuration, is modeled by forcing solute molecules in the feed that physically travel through the outer radial region of the membrane to virtually pass through a common PFR and then inlet CSTRs 1a, 2a, and 3a. The total average residence time of a solute molecule traversing this path is therefore modeled as the sum of the average residence times for the PFR and the three inlet CSTRs, while that for a solute molecule traveling down the column centerline is given by the sum of the residence times for the PFR and CSTR 1a only. Flow paths and average residence times in the eluent collection manifold are modeled in an equivalent manner. Different configurations of this three zone model are possible, as illustrated by the "diagonal" configuration shown in Fig. 2B, where solute molecules traveling through the outer radial region of the membrane now pass through a common inlet zone and then zone 3a. This configuration has the advantage that it provides a solute flow representation that more closely resembles the true flow path by explicitly accounting for sources of solute dispersion upstream of the feed distribution manifold and providing a unique hold-up volume for each zone. However, it requires an additional parameter

to do so, which unnecessarily complicates the model, and we therefore first focused on the standard ZRM configuration in Fig. 2A with the aim of minimizing both the number of regressed parameters and overall model complexity.

The required number of zones is optimized for the membrane chromatography module under investigation and should reflect a good compromise between complexity and accuracy of the model. An insufficient number of zones will violate the assumption that concentrations are radially homogeneous within a given zone, whereas an excessive number of zones result in insignificant concentration differences between the zones and an unnecessary complexity to the model.

Each virtual hold-up zone is modeled as a CSTR using the standard mass balance relation

$$\frac{dc^{CSTR}}{dt} = \frac{1}{\tau}(c_{in}^{CSTR} - c^{CSTR}) \tag{1}$$

where τ is the residence time of the tank and is equal to the ratio of the volumetric flow rate through the tank Q_i to the tank volume V_{CSTR}($\tau = Q_i/V_{CSTR}$); c_{in}^{CSTR} and c^{CSTR} are the solute concentrations in the tank inlet and outlet, respectively. A PFR modeled as

$$c_{out}^{PFR}(t) = \begin{cases} 0 & t < t_{lag} \\ c_{in}^{PFR} & t > t_{lag} \end{cases} \tag{2}$$

is placed in series within the flow network and accounts for an additional time lag that is uncoupled from the system dispersion. Here, the time lag, t_{lag}, is equal to V_{PFR}/Q. It should be noted that since the PFR provides a time lag but no dispersion, its relative position in the flow network is not important. Moreover, two or more such dead volumes within the network can be modeled with a single PFR. In the ZRM, the total time lag in the system is therefore accounted for by a single PFR placed before the tank/membrane network.

The membrane zones are modeled as isolated membrane stacks of defined cross-sectional area embedded in the network of stirred tanks. All experiments and model calculations reported in this work are for non-binding conditions, and solute convection and axial dispersion within a membrane stack are therefore modeled in the traditional manner with a simple continuity equation derived from a solute mass balance within an infinitesimal control volume [4,9,20]:

$$\frac{\partial c}{\partial t} + \nu\frac{\partial c}{\partial z} = D_a\frac{\partial^2 c}{\partial z^2} \tag{3}$$

Here $c(z,t)$ is the solute concentration in the mobile phase at time t and distance z from the column inlet, D_a is the axial dispersion coefficient, and ν is the interstitial velocity given by the ratio of the superficial velocity u to the membrane porosity ε. Danckwerts' boundary conditions are applied at the inlet ($z = 0$) and outlet ($z = L$) of each membrane stack [25]:

$$\nu \cdot c_{in}(t) = \nu \cdot c(0,t) - D_a\left.\frac{\partial c}{\partial t}\right|_{z=0} \tag{4}$$

$$\left.\frac{\partial c}{\partial z}\right|_{z=L} = 0 \tag{5}$$

Initial conditions assume a step concentration increase from $c_{in} = 0$ to $c_{in} = c_o$ at the root inlet of the tank network at time $t = 0$. As Eqs. (1)–(5) apply to flow-through conditions, they can be applied to any solute component introduced into the network.

The flexibility inherent in partitioning both the external hold-up volumes and column volume itself allows the ZRM to be applied to a variety of flow phenomena. In the membrane chromatography system modeled here, each zone within the membrane stack is treated identically and all flow non-uniformities are the result of the external volumes, but this does not necessarily have to be the case. Hydrodynamic, structural and mass-transfer properties within the column can be treated as zone dependent. For example, axial velocities and/or porosities can differ among column zones to account for the type of radial heterogeneity of interstitial velocities sometimes seen in packed bed chromatography due to wall effects [26–28].

2.2. Computational methods

The complete zonally segregated upstream hold-up volume, membrane stack and downstream hold-up volume network could be solved in a standard sequential manner by first solving the upstream hold-up volumes, then solving the membrane zones one by one with the upstream results giving the required initial conditions, and so on. However, that approach requires adaptive time stepping of the differential equation solver that necessarily complicates treatment of the initial and boundary conditions. We therefore chose to simultaneously solve the entire system of coupled model equations in a novel and much more computationally efficient manner as follows.

In the forward problem, where a breakthrough curve is computed for a given set of model parameters and specified column operating conditions, the partial differential equations for the membrane zones are first discretized along the axial coordinate by the method of lines [29]. The membrane zones are then coupled with the hold-up volume network as described in Appendix A, resulting in a large system of differential equations (ODE). The MATLAB solver *ode15s* [30] is used for time integration and must be restarted at any step discontinuity in the boundary conditions of the root tank.

With default settings the *ode15s* solver is predominantly occupied with numerically computing the system Jacobian, which is a matrix of size m by m that contains the partial derivatives of the right hand side of the nonlinear ODE system with respect to the m state variables of the spatially discretized model. We compute this matrix several orders of magnitude faster and more accurately by explicit differentiation of the corresponding model equations. Performance of the *ode15s* solver is further improved by a variable transformation that yields a diagonal mass matrix on the left hand side of the ODE system.

In the inverse problem, unknown model parameters are estimated from chromatogram data by repeatedly solving and updating the entire equation system using MATLAB's iterative optimization function *lsqnonlin* that uses an algorithm based on the interior-reflective Newton method [31,32]. Unknown parameters in the ZRM that must be regressed include those appearing in the PFR model (t_{lag}) and possibly the continuity equation (D_a) if a value is not already available. The ZRM as configured in Fig. 2A also requires values for two residence times per zone. This number can be halved if the chromatography module can be treated as axially symmetric, meaning the feed-distribution tank and eluent-collection tank within a given zone have identical average residence times (i.e. $\tau_{1a} = \tau_{1b}$, $\tau_{2a} = \tau_{2b}$, etc.). Additionally, as derived in Appendix A, a flow fraction Φ_i value is required for each additional zone beyond zone 1.

The need to develop the highly efficient solution algorithm described above arises because a typical system with one solute component, three zones, and 1000 axial knots is described by a system of $k = 1 \times 2 \times 3 \times 1000 = 6000$ equations, and one with three components, four zones and 1000 axial knots yields $k = 3 \times 3 \times 4 \times 1000 = 36{,}000$ equations. Since the computational effort increases nonlinearly with both the number of equations and unknown model parameters, a high computation speed is crucial for the practical applicability of the ZRM. The implementation of the computational algorithm described above enables a 2.20 GHz

desktop computer to solve the forward problem in *ca.* 10 s and the inverse optimization of 4 unknown parameters in less than 5 min.

3. Experimental

Mustang Q XT5 anion-exchange membrane chromatography modules (generously donated by Pall Inc. (East Hills, NY, USA)) containing modified hydrophilic polyethersulfone (PES) membranes were used in this study. The height and cross-sectional area of the stacked membrane bed in these modules are 2.20 mm and 22.06 cm^2, respectively, and the hold-up volume is 3.21 mL for both the feed-distribution and eluent-collection manifolds. The nominal pore size and porosity ε of the membranes is 0.8 μm and 0.70 ± 0.05 based on data provided by the manufacturer. The XT5 capsule was attached to an AKTAexplorer FPLC system controlled by Unicorn 4.12 software (Amersham Pharmacia, Uppsala, Sweden).

Breakthrough experiments were performed under non-binding conditions using 1 mg mL^{-1} ovalbumin (Sigma, Oakville, Canada) and a running buffer of 1 M NaCl in 25 mM Tris, pH 8.0 (Fischer Scientific, Ottawa, Canada). Experiments were performed at flowrates of 1.5, 5, 10 and 20 mL min^{-1}. The membrane stack was cleaned following the suggested protocol of the manufacturer using a 1 N NaOH solution followed by a wash with 1 M NaCl in 25 mM H_3PO_4 (Fischer Scientific, Ottawa, Canada).

4. Results and discussion

4.1. Comparison of existing hold-up volume models with experiment

Breakthrough curves under non-binding conditions for frontal loading of ovalbumin at four distinct flowrates (1.5, 5, 10 and 20 mL min^{-1}) were measured and first used to evaluate the performance of both a "base-case" stacked-membrane chromatography model that ignores all hold-up volume effects, as well as the more advanced "one-zone" model proposed by Roper and Lightfoot [17] that includes terms for estimating solute dispersion in the feed distributor (linear PFR to CSTR sequence), membrane stack (1D rate theory of chromatography), and eluent-collection manifold (linear CSTR to PFR sequence). Fig. 3A compares base-case model results to breakthrough data at 1.5 mL min^{-1} for the case where D_a is set to 7×10^{-11} m^2 s^{-1}, the diffusivity of ovalbumin in water at the column operating temperature [33]. This model calculation follows from the fact that the axial Peclet number *Pe* is generally quite large in stacked-membrane chromatography, and several studies have shown for such systems that the axial diffusion coefficient can be used in place of the axial dispersion coefficient with minimal error [e.g. 10]. Thus, we expect D_a to be near 7.0×10^{-11} m^2 s^{-1}, and this value is likewise in good agreement with available experimental values for membrane and monolithic columns (where, typically, $10^{-12} < D_a \leq 10^{-9}$ m^2 s^{-1}) [12,18,34,35] and appropriate correlations for estimating D_a from the physical structure and operating conditions of the column [36].As shown in Fig. 3A, the base-case model shows essentially no agreement with the breakthrough data when D_a is set equal to 7.0×10^{-11} m^2 s^{-1}, predicting almost no band broadening. As the experiments were conducted under non-binding conditions and low solute (ovalbumin) concentrations, the significant discrepancy between the base-case model and experiment cannot be attributed to dispersion effects related to slow kinetics of protein binding to or desorption from the stationary phase. The results therefore provide compelling evidence that solute dispersion within the inlet and outlet hold-up volumes makes a significant contribution to broadening of the breakthrough curve.

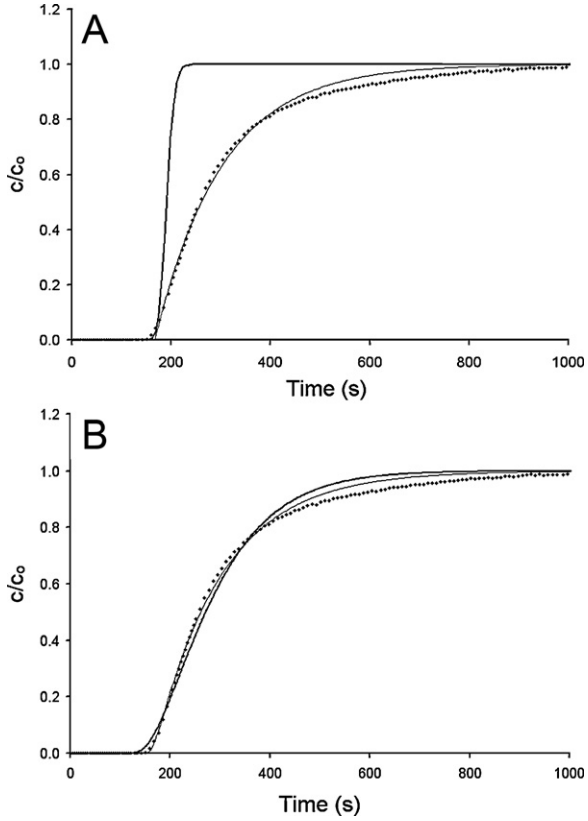

Fig. 3. Model fit of experimental breakthrough curves (●) for loading of ovalbumin (c_o = 1 mg mL^{-1}) on a Mustang XT5 module under non-binding conditions at a flow rate of 1.5 mL min^{-1} using: (A) the base-case membrane chromatography model which is comprised of a plug flow reactor in series with the 1D rate theory of chromatography; the bold line represents base-case model results for a D_a of 7×10^{-11} m^2 s^{-1} and the thin line for a regressed D_a of 1×10^{-4} m^2 s^{-1}; (B) the one-zone membrane chromatography model comprised of a plug flow reactor, a CSTR, the membrane stack and a second CSTR in series; the bold line represents model results for a D_a of 7×10^{-11} m^2 s^{-1} and the thin line for a regressed D_a of 1×10^{-5} m^2 s^{-1}.

Some amelioration of the base-case model error can of course be achieved by treating D_a as an apparent or lumped parameter that includes the contributions of the hold-up volumes to solute dispersion. This adaptation of the base case was therefore tested by globally regressing D_a to the complete set of breakthrough data. An improvement in model performance is observed (Fig. 3A), but significant discrepancies remain. Moreover, minimization of model error results in a regressed value of D_a (1.0×10^{-4} m^2 s^{-1}) that is clearly unrealistic from the perspective of specifically treating axial dispersion within the membrane stack, as it is at least 5 orders of magnitude higher than the expected value of D_a for this system.

The results in Fig. 3B show that the one-zone model of Roper and Lightfoot substantially addresses many of the shortcomings of the base-case model. When the flow rate is 1.5 mL min^{-1} and D_a is set to 7.0×10^{-11} m^2 s^{-1}, the one-zone model clearly captures the early stages of breakthrough much better than the base-case model. However, it does not accurately reproduce the later stages of breakthrough, including the slow approach to saturation of the membrane interstitial volume and associated hold-up volumes. These model errors, which also include the prediction of an initial breakthrough trend that is too shallow when compared to experiment, are similar to what has been previously reported for other one-zone type models [37]. The same errors are also observed at higher flow rates, though their magnitude decreases with increasing flow rate as indicated by the sum of the square of residuals data reported in Table 1.

Table 1
Comparison of the sum of the square of residuals between experimental breakthrough data for 1 mg mL^{-1} ovalbumin through a Mustang XT5 column under non-binding conditions and simulated breakthrough curves from the base-case, one-zone, two-zone and symmetric three-zone models at four distinct flowrates. D_a was set to 7×10^{-11} m^2 s^{-1}.

Flow rate (mL min^{-1})	Base case	1 zone[a]	2 zones (w and w/o symmetry)	3 zones (w/symmetry)
1.5	9.1374	0.5173	0.0034	0.0029
5	12.7519	0.3198	0.0077	0.0077
10	13.7395	0.0302	0.0074	0.0058
20	14.8522	0.0212	0.0133	0.0079

[a] Results computed using the model of Roper and Lightfoot [17] with $D_a = 7 \times 10^{-11}$ m^2 s^{-1}.

We note that a small reduction in model error can again be realized by treating D_a as a lumped adjustable parameter and regressing it to the complete set of breakthrough data (Fig. 3B). As before, however, the "optimal" value of the regressed D_a (1.0×10^{-5} m^2 s^{-1}) is completely unrealistic as an indicator of solute dispersion specifically within the membrane stack.

4.2. ZRM model configuration optimization and application

Flow-through conditions are best suited for determining the structure of the hold-up volume network in the ZRM, as the unknown system parameters are then limited to the residence times for the zonal CSTRs, the lag time for the required PFR, and D_a if it is not assumed equal to the diffusivity of ovalbumin. Dispersion effects associated with protein binding and elution are avoided and all other required model parameters are known, including the stacked membrane thickness and porosity, as well as the hold-up volumes of the inlet and outlet manifolds. In the XT5 module, the geometries of those two manifolds are simple mirror images, and the manifolds therefore share the same hold-up volume, 3.21 mL each. As a result, we expect the average solute residence time to be the same for the two manifolds.

We globally fit a number of configurations of the ZRM to the complete set of ovalbumin breakthrough data collected from the XT5 membrane chromatography module and then compared the sum of the square of residuals. Both the number of zones and the validity of the manifold symmetry approximation were tested to determine the ZRM configuration that best describes the experimental data with the minimum number of regressed parameters.

Table 1 reports sum of the square of residuals data for the fitting of several configurations of the standard ZRM to the breakthrough curves measured for frontal loading of ovalbumin at four different flow rates. All configurations of the ZRM tested resulted in significant improvement in model accuracy when compared to either the base-case or single-zone model. Indeed, as illustrated in Fig. 4A and B, calculated breakthrough curves from the simplest ZRM configuration tested (two zones) essentially superimpose the experimental data, and this result was true at all flow rates as evidenced by the sum of the squared residual values reported in Table 1. No change in ZRM performance was observed when the symmetry approximation was invoked, as should be expected from the geometry of the XT5 capsule. As a result, though the breakthrough data are also perfectly described by the ZRM configured either in two zones without symmetry or in three zones with tank symmetry (Table 1), the added complexity of those configurations is not required. The same arguments also made it unnecessary to evaluate the performance of the "diagonal" configuration of the ZRM shown in Fig. 2B.

Within the ZRM, the flow fraction through the outer zone, Φ_2, is independent of flow rate and was therefore directly regressed to the entire data set, giving a value of 0.26. This relatively low Φ_2 indicates that the ZRM can successfully address the deficiencies in the single-zone model to quantitatively capture solute dispersion in a stacked-membrane chromatography module by directing a relatively small percentage of the feed through zone 2. The values of the remaining parameters of the symmetric two-zone ZRM are

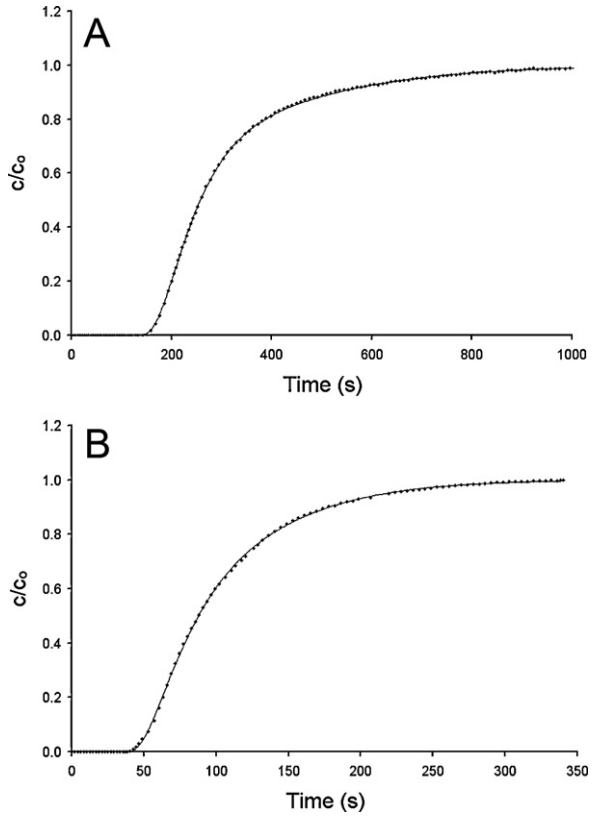

Fig. 4. Symmetric two-zone ZRM fit (solid line) of the experimental breakthrough data (●) for ovalbumin (c_o = 1 mg mL^{-1}) loaded on a Mustang XT5 module under non-binding conditions at a flow rate of (A) 1.5 mL min^{-1} and (B) 5 mL min^{-1}. D_a was 7×10^{-11} m^2 s^{-1} in all calculations.

reported in Table 2. All of these regressed times necessarily depend on flow rate since the associated hold-up volumes are constant. The product of the lag time t_{lag} and Q is a constant characteristic dead volume (*ca.* 0.38 mL) in accordance with the solution of the PFR model (Eq. (2)). Similarly, the residence time for each CSTR has a linear dependence on $1/Q$, as is required by the solution to Eq. (1). From a modeling perspective, what is important is that the values of and the disparity between the inner and outer zone residence times decrease with increasing Q. Solute dispersion effects associated with unequal flow paths through different regions of the

Table 2
Structural parameters for the symmetric two-zone ZRM configuration regressed from experimental breakthrough data for 1 mg mL^{-1} ovalbumin through a Mustang XT5 column under non-binding conditions at four distinct flowrates. D_a was set to 7×10^{-11} m^2 s^{-1}.

Flow rate (mL min^{-1})	t_{lag} (s)	τ_{inner} (s)	τ_{outer} (s)
1.5	15.25	45.4	125.3
5	4.57	20.5	37.6
10	2.29	11.5	18.8
20	1.14	6.1	9.4

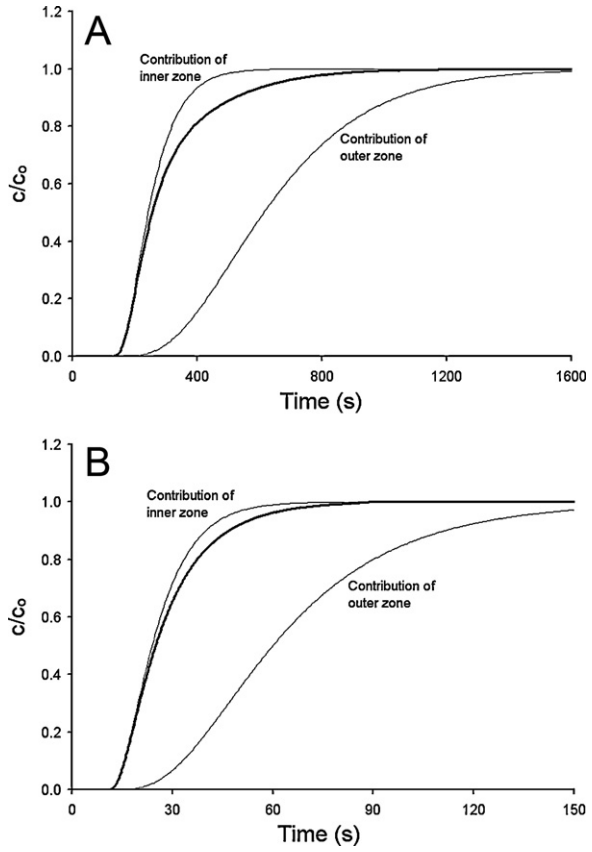

Fig. 5. Contributions of the inner and outer radial zones to elution band spreading of ovalbumin (c_o = 1.0 mg mL^{-1}) loaded on the XT5 module at (A) 1.5 mL min^{-1} or (B) 20 mL min^{-1}. The symmetric two-zone configuration of the ZRM was used for all calculations. The residence times of the inner and outer tanks were 45.4 s and 125.3 s, respectively, and the time lag was 15.25 s. D_a was set to 7×10^{-11} m^2 s^{-1}.

inlet and outlet manifolds are therefore predicted to be largest at low flow rates. All CSTR residence times approach zero near the highest flow rates recommended for operation of the module. As a result, differences between the symmetric two-zone ZRM and the single-zone model are diminished (Table 1), indicating that the ZRM effectively reduces to the simpler one-zone model of Roper and Lightfoot (but not the base-case model) at high *Q*.

4.3. Decomposition of system dispersion using the ZRM

In addition to accurate prediction of breakthrough, the ZRM provides the ability to decompose solute dispersion in order to analyze contributions taking place in each radial zone as a function of time and flow rate. Fig. 5 reports contributions to solute breakthrough from the inner and outer radial zones computed by the symmetric two-zone configuration of the ZRM for two different feed flow rates. The trends are qualitatively similar between the two flow rates. Significantly greater solute dispersion is predicted within zone 2 due to the longer average residence time of solute passing through the outer radial positions of each manifold. Breakthrough of solute from zone 2 is therefore delayed relative to that from zone 1 and, as a result, zone 2 does not contribute to the initial breakthrough of solute from the column. The ZRM therefore predicts a relatively steep initial breakthrough, as observed experimentally but not well described by previous models. The ZRM also predicts that when breakthrough from zone 1 is complete, the loading of zone 2 is less than half complete and the remaining slow approach to system saturation is fully determined by dispersion processes within zone 2 during the second half of its loading.

Table 3
Breakdown of ZRM predicted solute elution variance σ (s) for the 1.5 mL min^{-1} flow rate as a function of flow zone and flow elements within the zone.

Source of variance	Zone 1	Zone 2
Total	81.45 s	267.9 s
Feed distribution manifold	48.68 s	141.6 s
Membrane stack	1.62 s	0.33 s
Eluent collection manifold	31.15 s	126.0 s

For the 1.5 mL min^{-1} flow rate, the variance (σ) of the various dispersion processes within each zone are reported in Table 3 along with the total variance generated by the zone. For either zone, solute dispersion within the feed-distribution and eluent-collection manifolds accounts for at least 98% of the total dispersion. As should be expected for the commercial ion-exchange membranes used in this study, the membrane stack is highly efficient, offering an HETP of between 1 and 4 μm over the range of flow rates tested and contributing very little to the observed solute dispersion within the module. Indeed, the near step-change breakthrough curve (solid line) in Fig. 3A computed using the base-case model represents the degree of elution band broadening that would be expected if the external hold-up volumes provided no contribution to solute dispersion. It is interesting to note that the contribution of the membrane stack to the total solute dispersion is smaller in zone 2 (σ = 0.33 s) than in zone 1 (σ = 1.62 s) despite the fact that both D_a and v are the same within the two zones. This is due to differences in the shape and slope of the concentration gradient of solute entering the membrane stack from the two different zones of the feed distribution manifold. Due to the higher dispersion of solute exiting zone 2 of that manifold, d^2c/dz^2 in Eq. (3) takes on smaller values in general, resulting in lower dispersion within zone 2 of the membrane stack. Differences in initial conditions likewise account for the unique variance contributions made by each CSTR within the network.

The ZRM can also be used to explore operational space to identify system configurations or conditions where improvements in system performance might be realized. For example, Fig. 6 shows ZRM predictions of the effect on total solute dispersion, quantified here by the computed normalized second central moment ($\bar{\mu}_2/(\mu_1)^2$) where $\bar{\mu}_2$ equals σ^2 and μ_1 is the first moment, of changes to the values of Φ_2 and the column Peclet number *Pe*. When *Pe* > 100, which is true at 1.5 mL min^{-1} (*Pe* = 510) and typically the case in membrane chromatography, the contribution of the membrane to solute dispersion is negligible and the ZRM predicts that a sharpening of solute breakthrough can be achieved by engineering a set of inlet and outlet manifolds that serve to reduce Φ_2. As shown in Fig. 6, even a small decrease in Φ_2 could provide a significant improvement, as the ZRM predicts that $\bar{\mu}_2/(\mu_1)^2$ decreases rapidly with decreasing Φ_2 when *Pe* > 100.

The results in Fig. 6 also show that solute dispersion within the membrane stack is predicted to contribute significantly to broadening of the elution band when *Pe* drops to a value near 10 or lower. Thus, at a flow rate of 1.5 mL min^{-1}, a 2.2 mm thick membrane stack would contribute to the total variance if it were characterized by a D_a of 10^{-9} m^2 s^{-1}, which is at the high end of experimental D_a values reported for membrane and monolithic columns [12,18,31,32]. In this regime ($D_a \geq 10^{-9}$ m^2 s^{-1}), band broadening is predicted to depend strongly on D_a but, because the contributions of the inlet and outlet manifolds are reduced, show a much weaker dependence on Φ_2.

Operationally significant dispersion within the column can also be realized through an increase in column length. As shown in Fig. 7, an order of magnitude increase in the membrane bed height to 2.2 cm is predicted to increase $\bar{\mu}_2$ 3-fold (note the log scale), with further increases in bed height resulting in more significant

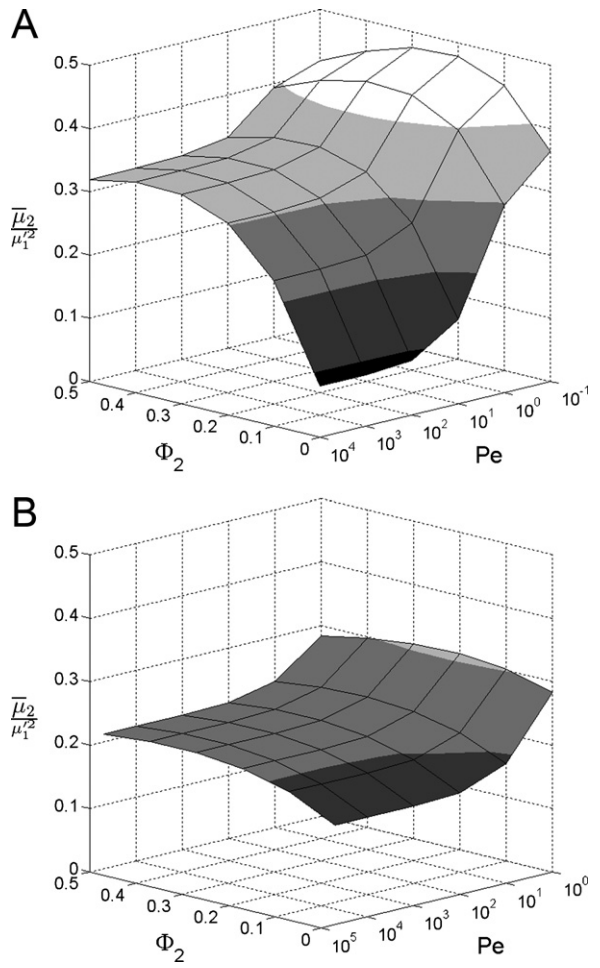

Fig. 6. Normalized second moment of ZRM simulated breakthrough curves as a function of Peclet number *Pe* and flow fraction through the outer zone (Φ_2) for the case where the column length is 2.2×10^{-3} m^2 and the flow rate is (A) 1.5 mL min^{-1} or (B) 20 mL min^{-1}. The symmetric two-zone configuration of the ZRM was used for all calculations.

increases in band broadening due to the membrane stack then making the dominant contribution to σ. When configured properly, the ZRM can therefore provide guidance on effective ways to increase column capacity by predicting the effects of increasing both bed diameter (which may increase hold-up volumes, associate residence times and number of zones) and bed height on column loading efficiency.

Finally, as shown in Section 4.2, the symmetric two-zone ZRM reduces to the one-zone model at high feed flow rates. In terms of the ZRM, this would mean that the total variance loses its dependence on Φ_2 with increasing flow rate. This is indeed the case (Fig. 6B). At a feed flow rate of 20 mL min^{-1}, $\bar{\mu}_2/(\mu_1)^2$ becomes nearly insensitive to Φ_2.

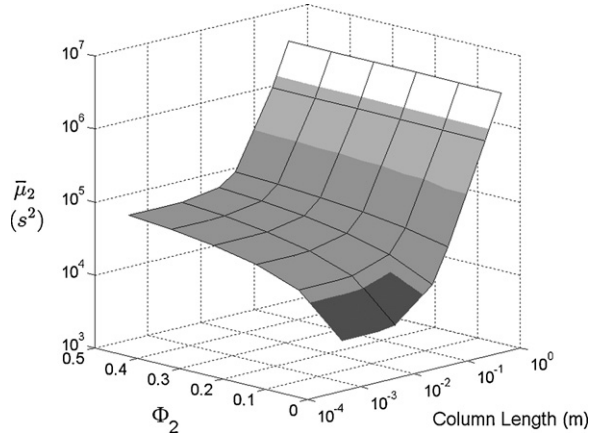

Fig. 7. Second central moment of ZRM simulated breakthrough curves as a function of column length and flow fraction through the outer zone (Φ_2) for the case where the flow rate is 1.5 mL min^{-1} and D_a is 7×10^{-11} m^2 s^{-1}.

5. Conclusions

In stacked-membrane chromatography the large column diameter to length ratio naturally leads to variations in solute residence times within the feed-distribution and eluent-collection manifolds. The ZRM accounts for these unequal flow paths by radially partitioning the membrane stack and associated hold-up volumes into virtual zones. By fitting the model to a small set of breakthrough data obtained under non-binding conditions – thus avoiding any dispersion effects associated with protein adsorption and desorption – an appropriate ZRM structure can be identified and then used both to quantitatively match breakthrough data over a range of operating conditions, including those flow rates where previous membrane-chromatography models fail, and to decompose the breakthrough data to identify and possibly correct major sources of band broadening within the system. The results highlight the importance of proper design of the external hold-up volumes, especially in systems where the membrane volume is equal to or less than the external hold-up volumes.

In a follow-up publication, we use the ZRM to characterize stacked-membrane chromatography under binding conditions to permit the regression of binding kinetics parameters and the proper form of the adsorption isotherm from limited data, the prediction of breakthrough curves, and the optimization and scale-up of a separation from data acquired on the scaled-down XT5 module. Treating the hydrodynamic and adsorption effects separately enables scale-up to proceed in an economical and efficient manner. The zonal arrangement as well as tank sizes and flow ratios are first determined at scale following the procedure outlined in this work. The binding parameters and isotherm determined from the scaled-down device are directly transferable across scales and geometries as they are independent of the flow effects in the external hold up volumes. This greatly reduces the costs associated with optimizing large scale chromatography modules using the ZRM.

Acknowledgements

C.A.H. receives salary support as the Canada Research Chair in Interfacial Biotechnology. This work was supported by grants from the Natural Sciences and Engineering Research Council of Canada (NSERC) and Canadian Institutes of Health Research (CIHR).

Appendix A.

The sum of volumetric flow rates Q_i through the individual zones equals the overall volumetric flow rate Q through the chromatography module. We therefore may define flow fractions $\Phi_i = Q_i/Q$ which are independent of the overall volumetric flow rate Q and contain one degree of freedom less than the corresponding volumetric flow rates Q_i. Together, the flow fractions and the interstitial velocities are required to determine the size of each membrane zone since a small zone with fast interstitial flow can have the same volumetric flow rate as a large zone with slow interstitial flow.

In a network of CSTRs the number of outflows from a given tank is irrelevant to the mathematical description. If one tank feeds another in the physical model, the corresponding equations are

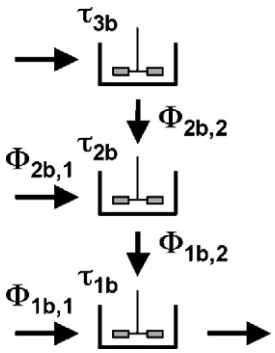

Fig. A1. Junction of flows through three zones in a cascade of CSTRs.

coupled by taking the concentration within the feeding tank as the inlet concentration of the fed tank. The same rule holds when a tank feeds a membrane zone. Downstream of the membrane stack however, the model includes tanks with multiple inflows (see Fig. 2). A tank with j inflows is mathematically described by an instance of Eq. (A.1).

$$\frac{\partial c^{CSTR}}{\partial t} = \sum_{i=1}^{j} \frac{c_{in,i}^{CSTR}}{\tau_i} - \frac{c^{CSTR}}{\tau} \tag{A.1}$$

where

$$\frac{1}{\tau} = \sum_{i=1}^{j} \frac{1}{\tau_i} \tag{A.2}$$

Here c^{CSTR} denotes the concentration in the respective tank, c_{in}^{CSTR} the corresponding inlet concentration and τ the residence time.

A set of flow fractions must be defined for each tank with more than one inlet. Fig. A1 illustrates this situation in more detail and represents the collector tanks from Fig. 2A. The set Φ_1 to Φ_3 with $\Phi_1 + \Phi_2 + \Phi_3 = 1$ refers to the flow fraction through each zone, while the sets $\Phi_{1b,1}$ and $\Phi_{1b,2}$ with $\Phi_{1b,1} + \Phi_{1b,2} = 1$ as well as $\Phi_{2b,1}$ and $\Phi_{2b,2}$ with $\Phi_{2b,1} + \Phi_{2b,2} = 1$ refer to the inlets of tanks 1b and 2b, respectively. An instance of Eq. (A.1) is set up for each of these tanks with residence times $1/\tau_{1b,1} + 1/\tau_{1b,2} = 1/\tau_{1b}$ and $1/\tau_{2b,1} + 1/\tau_{2b,2} = 1/\tau_{2b}$, and with flow fractions $\Phi_{1b,i} = \tau_{1b}/\tau_{1b,i}$ and $\Phi_{2b,i} = \tau_{2b}/\tau_{2b}$, for $1 \le i \le 2$. The flow fractions through the membrane zones are then uniquely determined by $\Phi_1 = \Phi_{1b,1}$, $\Phi_2 = \Phi_{1b,2} \cdot \Phi_{2b,1}$ and $\Phi_3 = \Phi_{1b,2} \cdot \Phi_{2b,2}$. Analogous relations can be derived for complex networks with more membrane zones or with exchange flows between the tanks.

References

[1] E. Klein, J. Membr. Sci. 179 (2000) 1.
[2] D.K. Roper, E.N. Lightfoot, J. Chromatogr. A 702 (1995) 3.
[3] R. Ghosh, J. Chromatogr. A 952 (2002) 13.
[4] J. Thömmes, M.-R. Kula, Biotechnol. Prog. 11 (1995) 357.
[5] C. Charcosset, Biotechnol. Adv. 24 (2006) 482.
[6] R. Van Reis, A. Zydney, J. Membr. Sci. 297 (2007) 16.
[7] A. Saxena, B.P. Tripathi, M. Kumar, V.K. Shahi, Adv. Colloid Interface Sci. 145 (2009) 1.
[8] J.X. Zhou, T. Tressel, U. Gottschalk, F. Solamo, A. Pastor, S. Dermawan, S.T. Hong, O. Reif, J. Mora, F. Hutchison, M. Murphy, J. Chromatogr. A 1134 (2006) 66.
[9] S.-Y. Suen, M.R. Etzel, Chem. Eng. Sci. 47 (1992) 1355.
[10] K.G. Briefs, M.-R. Kula, Chem. Eng. Sci. 47 (1992) 141.
[11] H.C. Liu, J.R. Fried, AIChE J. 40 (1994) 40.
[12] K.H. Gebauer, J. Thömmes, M.R. Kula, Chem. Eng. Sci. 52 (1997) 405.
[13] S.-Y. Suen, M.R. Etzel, J. Chromatogr. A 686 (1994) 179.
[14] C. Boi, S. Dimartino, G.C. Sarti, J. Chromatogr. A 1162 (2007) 24.
[15] J. Wang, F. Dismer, J. Hubbuch, M. Ulbricht, J. Membr. Sci. 320 (2008) 456.
[16] H. Yang, M.R. Etzel, Ind. Eng. Chem. Res. 42 (2003) 890.
[17] D.K. Roper, E.N. Lightfoot, J. Chromatogr. A 702 (1995) 69.
[18] F.T. Sarfert, M.R. Etzel, J. Chromatogr. A 764 (1997) 3.
[19] H. Yang, M. Bitzer, M.R. Etzel, Ind. Eng. Chem. Res. 38 (1999) 4044.
[20] R.M. Montesinos-Cisneros, J. de la Vega Olivas, J. Ortega, R. Guzmán, A. Tejeda-Mansir, Biotechnol. Prog. 23 (2007) 881.
[21] T. Vicente, M.F.Q. Sousa, C. Peixoto, J.P.B. Mota, P.M. Alves, M.J.T. Carrondo, J. Membr. Sci. 311 (2008) 270.
[22] E.N. Lightfoot, A.M. Athalye, J.L. Coffman, D.K. Roper, T.W. Root, J. Chromatogr. A 707 (1995) 45.
[23] R. Ghosh, T. Wong, J. Membr. Sci. 281 (2006) 532.
[24] E. von Lieres, J. Wang, M. Ulbricht, Chem. Eng. Technol. 33 (2010) 960.
[25] J.A. Barber, J.D. Perkins, R.W.H. Sargent, Chem. Eng. Sci. 53 (1998) 1463.
[26] T. Farkas, G. Guiochon, Anal. Chem. 69 (1997) 4592.
[27] T. Yun, G. Guiochon, J. Chromatogr. A 760 (1997) 17.
[28] R.A. Shalliker, B.S. Broyles, G. Guiochon, J. Chromatogr. A 888 (2000) 1.
[29] W.E. Schiesser, The Numerical Method of Lines, Academic Press, San Diego, 1991.
[30] L.F. Shampine, M.W. Reichelt, SIAM J. Sci. Comput. 18 (1997) 1.
[31] T.F. Coleman, Y. Li, SIAM J. Opt. 6 (1996) 418.
[32] T.F. Coleman, Y. Li, Math. Prog. 67 (1994) 189.
[33] M.T. Tyn, T.W. Guzek, Biotechnol. Bioeng. 35 (1990) 327.
[34] J. Yun, H. Kirsebom, I.Y. Galaev, B. Mattiasson, J. Sep. Sci. 32 (2009) 2601.
[35] F. Gritti, W. Piatkowski, G. Guiochon, J. Chromatogr. A 983 (2003) 51.
[36] C.L. de Ligny, Chem. Eng. Sci. 47 (1970) 253.
[37] J.E. Kochan, Y.-J. Wu, M.R. Etzel, Ind. Eng. Chem. Res. 35 (1996) 1150.